King's Research Portal

Document Version
Publisher's PDF, also known as Version of record

[Link to publication record in King's Research Portal](#)

Altered small-world topology of structural brain networks in infants with intrauterine growth restriction and its association with later neurodevelopmental outcome

Dafnis Batalle [a,b], Elisenda Eixarch [a,b], Francesc Figueras [a,b], Emma Muñoz-Moreno [a,b], Nuria Bargallo [c], Miriam Illa [a,b], Ruthy Acosta-Rojas [a,b], Ivan Amat-Roldan [a,b], Eduard Gratacos [a,b,*]

[a] Department of Maternal–Fetal Medicine, Institut Clinic de Ginecologia, Obstetricia i Neonatologia (ICGON),
Hospital Clinic and Institut d'Investigacions Biomediques August Pi i Sunyer (IDIBAPS), University of Barcelona, Barcelona, Spain
[b] Centro de Investigacion Biomedica en Red de Enfermedades Raras (CIBERER), Barcelona, Spain
[c] Department of Radiology, Centre de Diagnostic per la Imatge, Hospital Clinic, Barcelona, Spain

ABSTRACT

Intrauterine growth restriction (IUGR) due to placental insufficiency affects 5–10% of all pregnancies and it is associated with a wide range of short- and long-term neurodevelopmental disorders. Prediction of neurodevelopmental outcomes in IUGR is among the clinical challenges of modern fetal medicine and pediatrics. In recent years several studies have used magnetic resonance imaging (MRI) to demonstrate differences in brain structure in IUGR subjects, but the ability to use MRI for individual predictive purposes in IUGR is limited. Recent research suggests that MRI in vivo access to brain connectivity might have the potential to help understanding cognitive and neurodevelopment processes. Specifically, MRI based connectomics is an emerging approach to extract information from MRI data that exhaustively maps inter-regional connectivity within the brain to build a graph model of its neural circuitry known as brain network. In the present study we used diffusion MRI based connectomics to obtain structural brain networks of a prospective cohort of one year old infants (32 controls and 24 IUGR) and analyze the existence of quantifiable brain reorganization of white matter circuitry in IUGR group by means of global and regional graph theory features of brain networks. Based on global and regional analyses of the brain network topology we demonstrated brain reorganization in IUGR infants at one year of age. Specifically, IUGR infants presented decreased global and local weighted efficiency, and a pattern of altered regional graph theory features. By means of binomial logistic regression, we also demonstrated that connectivity measures were associated with abnormal performance in later neurodevelopmental outcome as measured by Bayley Scale for Infant and Toddler Development, Third edition (BSID-III) at two years of age. These findings show the potential of diffusion MRI based connectomics and graph theory based network characteristics for estimating differences in the architecture of neural circuitry and developing imaging biomarkers of poor neurodevelopment outcome in infants with prenatal diseases.

© 2012 Elsevier Inc. All rights reserved.

Introduction

Intrauterine growth restriction (IUGR) due to placental insufficiency affects 5–10% of all pregnancies and it is a leading cause of fetal morbidity and mortality (Jarvis et al., 2003; Kady and Gardosi, 2004). Reduction of placental blood flow results in sustained exposure to hypoxemia and undernutrition (Baschat, 2004) and this has profound consequences on the developing brain (Rees et al., 2011). A substantial number of studies have described associations between IUGR and short (Bassan et al., 2011; Figueras et al., 2009) and long-term neurodevelopmental and cognitive dysfunctions (Bassan et al., 2011; Eixarch et al., 2008; Feldman and Eidelman, 2006; Geva et al., 2006a,b; Leitner et al., 2007; McCarton et al., 1996; Scherjon et al., 2000). Prediction of neurodevelopmental outcomes in IUGR is among the clinical challenges of modern fetal medicine and pediatrics. This goal is currently hampered by the limited understanding of the brain reorganization processes leading to poor neurodevelopment in IUGR children and the lack of suitable imaging biomarkers in fetal or early life.

In recent years several studies have used magnetic resonance imaging (MRI) to demonstrate differences in brain structure in IUGR subjects. Studies in term neonates have reported decreased volume in gray matter (Tolsa et al., 2004) and hippocampus (Lodygensky et al., 2008), and major delays in cortical development, with discordant patterns of gyrification and a pronounced reduction in cortical expansion (Dubois et al., 2008). Persistence of structural changes at 1-year of age has been recently reported demonstrating reduced volumes of gray matter (GM) in the temporal, parietal, frontal, and insular regions (Padilla et al., 2011) and decrease in fractal dimension of both gray and white matter (WM) which correlate with specific developmental difficulties (Esteban et al., 2010). Despite these studies are useful to demonstrate disease-related differences, the ability to use MRI information to generate individual predictive biomarkers in IUGR is limited.

Recent research suggests that MRI in vivo access to brain connectivity might help understanding cognitive and neurodevelopment processes (Sporns et al., 2005). Connectomics (Hagmann, 2005) is an emerging approach to extract information from different modalities, including MRI data, exhaustively mapping inter-regional connectivity within the brain to build a graph model of its neural circuitry known as brain network or connectome (Bullmore and Sporns, 2009; Sporns et al., 2005). Particularly, connectomics extracts a number of "image features" after intensive processing that integrates structural information of the individual, related to anatomical brain regions and neuronal connectivity, to compute adjacency matrices that represent brain networks or graph models of a particular subject brain. Connectomics provides a framework to compare architecture of brain circuits among different individuals in a direct and elegant manner. In order to assess brain organization, graph theory tools have been proposed to allow quantifying brain network infrastructure, integration and segregation of the global functioning of a brain network (Rubinov and Sporns, 2009). Of further interest is the ability to explore regional differences by assessing graph theory characteristics of the regional networks associated to a given region.

Connectomics has been successfully utilized in different sets of data, including functional MRI, structural MRI and diffusion MRI, to report altered group connectivity parameters in adults and adolescents undergoing diseases such as schizophrenia (Alexander-Bloch et al., 2010; Bassett et al., 2008; Liu et al., 2008), Parkinson's disease (Wu et al., 2009), Alzheimer's disease (He et al., 2008, 2009a; Lo et al., 2010), attention deficit hyperactivity disorder (Wang et al., 2009), and in non-clinical samples as in the study of synesthesia (Hänggi et al., 2011). These studies suggest the potential of MRI based connectomics to develop biomarkers for disease diagnosis and treatment effects monitoring. Among the above MRI modalities diffusion imaging can be of particular interest for the study of the developing brain. Diffusion MRI allows non-invasively assessing in-vivo WM fiber orientation in the brain. In recent years diffusion MRI based connectomics has been used to construct structural brain networks in healthy populations (Gong et al., 2009; Hagmann et al., 2008; Iturria-Medina et al., 2008), being its network properties associated with sex and brain size (Yan et al., 2010), intelligence (Li et al., 2009) and specific cognitive abilities in old age (Wen et al., 2011) and to report altered group network topology features in Alzheimer's disease (Lo et al., 2010; Wee et al., 2010), multiple sclerosis (Shu et al., 2011), schizophrenia (Wang et al., 2012) and early blindness (Shu et al., 2009). Connectomics from diffusion MRI has been applied to assess normal development of the human brain during childhood and adolescence, including subjects from 2 to 18 years of age (Hagmann et al., 2010). Diffusion MRI connectomics in younger children has been used to study a healthy longitudinal cohort of 2 weeks, 1 year and 2 years of age (Yap et al., 2011), but no studies in infants with perinatal conditions have been conducted.

In the present study, we evaluated the hypothesis that diffusion MRI based connectomics could determine quantifiable changes resulting from the existence of brain reorganization in children who suffered IUGR. We used diffusion MRI based connectomics to obtain structural brain networks in one year old infants with and without growth restriction. We analyzed global and regional graph theory features of brain networks explored in previous studies such as infrastructure, integration, segregation and centrality. We evaluated the ability of diffusion MRI based connectomics to demonstrate group differences in global brain network features and localize altered regional networks. Finally, we also explored whether brain network features at one year would be associated with neurodevelopmental outcome at two years of age.

Methods

Subjects

This study was part of a larger prospective research program on IUGR involving fetal assessment and short- and long-term postnatal follow-up at Hospital Clinic (Barcelona-Spain). The study design involved recruitment of a consecutive sample of 83 fetuses: 42 IUGR singleton infants and 41 control fetuses appropriate for gestational age. All individuals were born between October 2007 and November 2009. IUGR was defined as a fetal estimated weight below 10th centile according to local reference standards (Figueras et al., 2008) confirmed at birth. Control subjects were defined as fetuses with fetal estimated weight between the 10th and 90th customized centiles according to local reference (Figueras et al., 2008) confirmed at birth and were sampled from our general pregnant women population during the same period. Pregnancies were dated according to the first-trimester crown-rump length measurements (Robinson and Fleming, 1975). Infants with chromosomal, genetic, or structural defects and signs of intrauterine infection or neonatal early onset sepsis as defined by positive blood culture within the first 72 h of life were excluded from this study. Neonatal data were prospectively recorded including: gestational age (GA), birth weight, gender, Apgar at 5 min, umbilical artery pH and neonatal complications including late-onset sepsis, necrotizing enterocolitis and chronic lung disease (defined as oxygen need at 36 weeks postmenstrual age). Maternal education was recorded as low, intermediate or high educational level. Maternal smoking status during pregnancy and breastfeeding were also recorded. Growth parameters (weight, length, body mass index and head circumference) were recorded at 12 months and were normalized for local standards (Sobradillo et al., 2004). The study protocol was approved by the local Ethics Committee, and written informed consent was obtained from the parents or legal guardians of all participants.

Neurodevelopmental assessment

Neurodevelopmental outcome was assessed at 21 months of corrected age (CA) (± 3 months) with the Bayley Scale for Infant and Toddler Development, Third edition (BSID-III), which evaluates five distinct scales: cognitive; language; motor; socio-emotional behavior; and adaptive behavior. The scales have scores with a mean of 100 and S.D. of 15. Abnormal BSID-III was defined as a score below 85 in any of the five different scales (Anderson et al., 2010). All developmental examinations were performed by a single trained psychologist examiner with previous experience with the BSID-III. The examiner was not informed about the infant medical history.

MRI data acquisition

Children were scanned at 12 ± 2 months CA, during natural sleep. Structural MRI and diffusion MRI were performed using a TIM TRIO 3.0 T whole body MR scanner (Siemens, Germany). Diffusion images were acquired by using a single-shot Echo-Planar Imaging (SE-EPI) sequence covering 30 diffusion directions with a b-value of 1000 s/

mm^2. All acquired images covered the whole brain, with 3-mm slice thickness with no interslice gap, 40 axial slices and in-plane acquisition matrix of 122×122 with a field of view (FoV) set to 200×200 mm which resulted in a voxel dimension of $1.64 \times 1.64 \times 3$ mm^3, repetition time (TR) = 9300 ms, echo time (TE) = 94 ms. An additional image without diffusion weight (b = 0 s/mm^2) was also acquired. High resolution structural T1 weighted images were obtained by a Magnetization Prepared Rapid Acquisition Gradient Echo (MPRAGE) sequence with the following parameters: 0.9-mm slice thickness with no interslice gap, 192 sagittal slices, in-plane acquisition matrix of 256×256, FoV = 220×220 mm^2, which resulted in a voxel dimension of $0.86 \times 0.86 \times 0.9$ mm^3, TR = 2050 ms, TE = 2.41 ms and inversion time (TI) = 1050 ms. All acquired MRI structural and diffusion images were visually inspected for apparent or aberrant artifacts, and subjects excluded accordingly. In addition, structural T2 weighted images were also acquired in order to exclude WM abnormalities. Diffusion weighted images were corrected for eddy currents effects and simple head motions using FMRIB's Diffusion Toolbox (FSL 4.1; www.fmrib.ox.ac.uk/fsl).

White matter brain network construction

The methodology to compute individual connectivity based on MRI acquisitions was composed by a comprehensive integration of standard protocols (Fig. 1).

White matter, gray matter and cerebrospinal fluid segmentation

3D structural volumes were segmented into WM, GM and cerebrospinal fluid (CSF) using the unified segmentation model (Ashburner and Friston, 2005) available at the SPM software (SPM8 release, www.fil.ion.ucl.ac.uk/spm/). The SPM8 software was slightly modified to better fit an infant brain. Since the original software package uses default tissue probability maps derived from adult brains, we replaced the original templates by specific one year old infant a priori tissue probability maps (Altaye et al., 2008) (available at irc.cchmc.org/software/infant.php) which could fit better with the anatomical brain features of the patients included in the study.

Structural 3D volume of each subject was registered to its correspondent b$_0$ volume (in the diffusion native space) using IRTK (www.
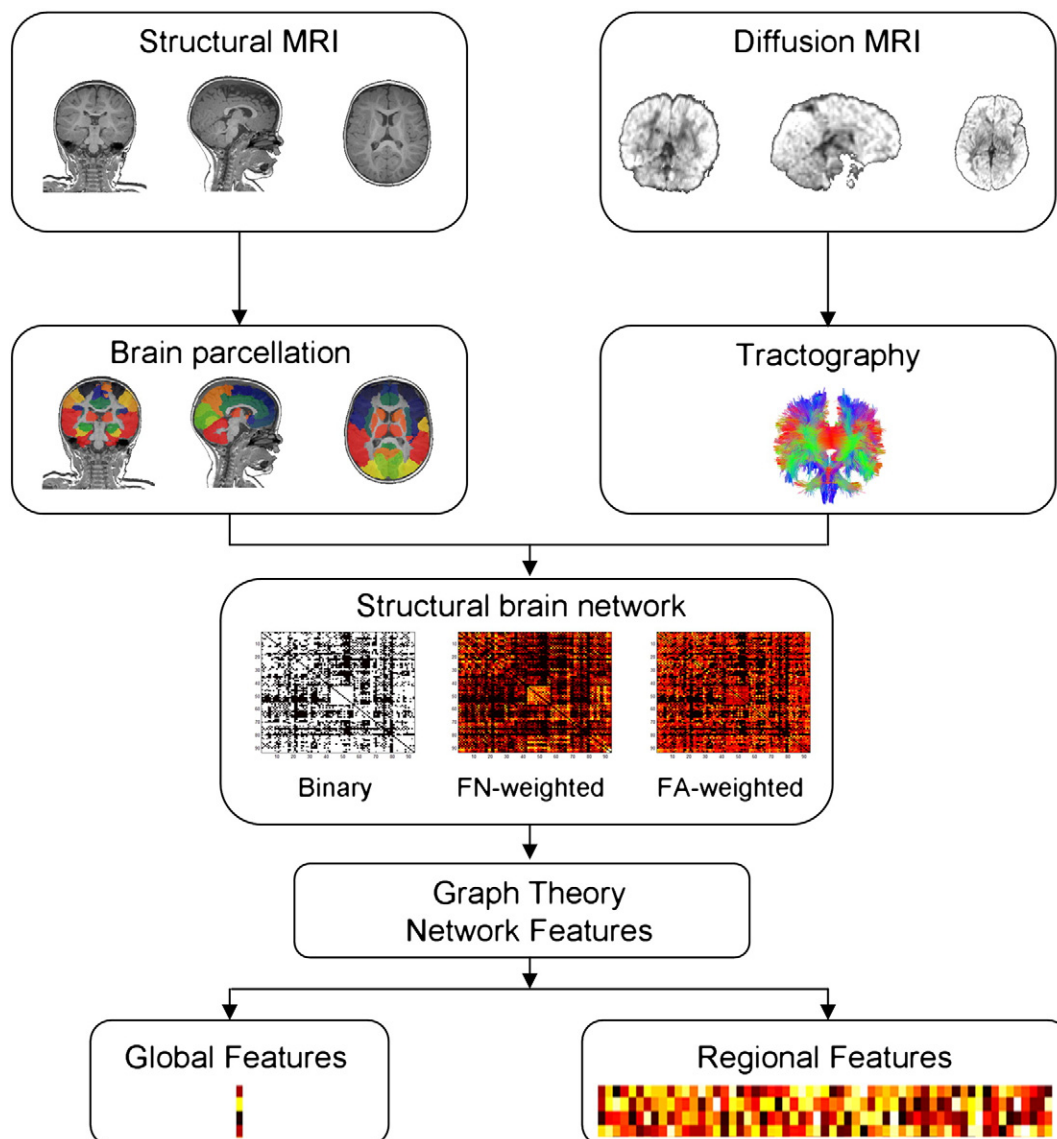
Fig. 1. Methodological scheme. By means of automatic parcellation and tractography, structural and diffusion MRI data of each subject is integrated into adjacency matrices (connectomes) and global and regional brain network features are extracted.

doc.ic.ac.uk/~dr/software/) to perform a 3D voxel-based affine registration maximizing normalized mutual information of each pair of images (Maes et al., 1997; Studholme et al., 1999). The transformation obtained for each subject was used to transform WM, GM and CSF to the diffusion native space.

Network node definition

Anatomical Automatic Labeling (AAL) atlas (Tzourio-Mazoyer et al., 2002), has recently been adapted to a one year old population (Shi et al., 2011) and is available online (http://bric.unc.edu/ideagroup/free-softwares/unc-infant-0-1-2-atlases/). In order to automatically parcellate each subject brain using this atlas, we have used a customized software implementing a consistent version (Tristan-Vega and Arribas, 2007) of a block matching algorithm (Warfield et al., 2002), allowing to obtain an elastic transformation matching the template with each subject anatomical T1 volume. The labels of AAL atlas were propagated to each structural MRI acquisition of our subjects using this elastic transformation, and transformed to diffusion native space with the previously calculated affine transformation. Discrete labeling values were preserved by nearest neighbor interpolation for both transformations. The original atlas is composed by 90 cortical and sub-cortical regions and 16 cerebellar regions. In order to simplify the analysis, we merged the cerebellar regions into right cerebellum, left cerebellum and vermix, resulting into a total of 93 regions per subject brain (Table 1), each of which corresponded to a node in the brain network.

Table 1
Regions of interest used as nodes in structural brain networks, corresponding to the regions defined in AAL atlas.

Anatomical regions	Label	Anatomical regions	Label
Precentral gyrus	PRE	Lingual gyrus	LING
Superior frontal gyrus, dorsolateral	F1	Superior occipital gyrus	O1
Superior frontal gyrus, orbital	F1O	Middle occipital gyrus	O2
Middle frontal gyrus	F2	Inferior occipital gyrus	O3
Middle frontal gyrus, orbital part	F2O	Fusiform gyrus	FUSI
Inferior frontal gyrus, opercular part	F3OP	Postcentral gyrus	POST
Inferior frontal gyrus, triangular part	F3T	Superior parietal gyrus	P1
Inferior frontal gyrus, orbital part	F3O	Inferior parietal, but supramarginal and angular gyri	P2
Rolandic operculum	RO	Supramarginal gyrus	SMG
Supplementary motor area	SMA	Angular gyrus	AG
Olfactory cortex	OC	Precuneus	PQ
Superior frontal gyrus, medial	F1M	Paracentral lobule	PCL
Superior frontal gyrus, medial orbital	F1MO	Caudate nucleus	CAU
Gyrus rectus	GR	Lenticular nucleus, putamen	PUT
Insula	IN	Lenticular nucleus, pallidum	PAL
Anterior cingulate and paracingulate gyri	ACIN	Thalamus	THA
Median cingulate and paracingulate gyri	MCIN	Heschl gyrus	HES
Posterior cingulate gyrus	PCIN	Superior temporal gyrus	T1
Hippocampus	HIP	Temporal pole: superior temporal gyrus	T1P
Parahippocampal gyrus	PHIP	Middle temporal gyrus	T2
Amygdala	AMYG	Temporal pole: middle temporal gyrus	T2P
Calcarine fissure and surrounding cortex	V1	Inferior temporal gyrus	T3
Cuneus	Q	Cerebellum	CER
		Vermis	VER

White matter tractography

A deterministic tractography was performed for each subject diffusion data using a diffusion tensor imaging (DTI) based fiber tracking algorithm with log-Euclidean metrics (Fillard et al., 2007), available on MedINRIA 1.9 (www-sop.inria.fr/asclepios/software/MedINRIA/). A relatively low Fractional Anisotropy (FA) threshold of 0.1 was chosen as stopping criterion for the fiber tract algorithm in order to ensure that the fiber tracts invade the WM–GM interface. Note that the preprocessing prior to the tractography includes a joint tensor field estimation and regularization that reduce the noise in the estimated DTI volume used to compute the tractography (Fillard et al., 2007).

Network edge definition

Tractography generated in the previous step was integrated to the anatomical parcellation in diffusion space in order to construct the inter-cortical brain network. Similarly to Shu et al. (2011), we characterized each brain network with a binary adjacency matrix and two weighted matrices. Specifically, two nodes (regions) i and j were considered to be connected by an edge e_{ij}, when there exist at least one fiber bundle f with end-points in i and j WM–GM interface, with self-loops excluded. Some authors proposed to establish a threshold of a minimum number of fiber bundles connecting two ROIs to consider them connected by an edge (Li et al., 2009; Lo et al., 2010; Shu et al., 2009, 2011) in order to minimize false positives that may be introduced into individual networks due to the noisy nature of the acquisitions. However, it has been suggested that the use of different thresholds does not significantly influence the resulting network analysis in case–control studies (Li et al., 2009; Lo et al., 2010; Shu et al., 2011). Analyses applying a fiber threshold from 1 to 5 fiber bundles were performed, but we focused in the analysis of unthresholded networks, as it was considered to be a more objective criterion preserving the whole structure of the connectivity in each individual. Network edge weights were defined according to two different criteria: fiber number (FN) connecting each pair of regions, and mean FA along all the fibers connecting a pair of region, hence obtaining two weighted adjacency matrices in addition to the binary one.

Network analysis

Network analysis of structural brain networks enables a refinement of image features obtained from MRI. As brain networks are defined by nodes (regions) and edges that connect pairs of nodes, which are represented mathematically by adjacency matrices or graphs (Hagmann et al., 2007), it is possible to characterize every subject structural brain network with a set of graph theory measures (or equivalently, network features) that summarize the behavior of a network. Particularly, we characterized each of the three brain network classes computed for each subject (binary, FN-weighted and FA-weighted) at two levels: global and regional.

At a global level, network infrastructure (i.e. mean degree), segregation (i.e. local efficiency) and integration (i.e. global efficiency) were characterized by means of standard measures as described in Supplementary material. At a regional level, a node based analysis was performed to extract the way in which these elements were embedded in the network (Rubinov and Sporns, 2009) by a set of network features of each node and its associated regional network. In that sense, in the network of a subject, a regional network associated to a given node was defined as the new network composed by the neighbors of that node, that is, by the nodes that are connected to that node. Nodes i and j are considered neighbors in a network if there exist an edge e_{ij} that connect both nodes (Rubinov and Sporns, 2009). Therefore, the definition of regional networks was based on its network topology, that is, in the connections among regions no matter how distant were from each other, not in anatomical and/or contiguity criteria. Specifically, regional network infrastructure (i.e., nodal degree), regional

network functional integration (i.e., nodal efficiency), and centrality of the node (i.e., betweenness centrality) were assessed.

In summary, the global level analysis included: average degree, global efficiency and local efficiency of each subject structural brain network. Regional level analysis included nodal degree, betweenness centrality and nodal efficiency of all the nodes of each subject structural brain network. For both global and regional network features the definitions of Rubinov and Sporns (2009) were applied and Brain Connectivity Toolbox (Rubinov and Sporns, 2009) was used to calculate most of them. Global, local and nodal efficiencies were calculated in both their binary and weighted versions according to the brain network considered.

Small-worldness

"Small-world" network model was originally characterized by (Watts and Strogatz (1998)), relating network clustering coefficient C_p, and characteristic path length L_p. According Watts and Strorgatz criterion, small-world networks have L_p comparable to a random equivalent network but a higher C_p. Specifically, C_p and L_p of each network were compared with equivalent random networks with the same size and degree distribution.

A more general criterion that characterizes small-world networks in terms of efficiency was also used. Following these criteria, a network can be considered to follow a small-world model if it accomplishes both following conditions (Achard and Bullmore, 2007):

$$E_{glob}^{latt} < E_{glob} < E_{glob}^{rand} \text{ and } E_{loc}^{rand} < E_{loc} < E_{loc}^{latt}$$

where E_{glob}^{latt} and E_{loc}^{latt} are the global and local efficiency of a lattice (regular) equivalent of the network, and E_{glob}^{rand} and E_{loc}^{rand} are the global and local efficiency of an equivalent random network. It can be seen as a network with an optimal balance between local processing and global integration (Sporns and Tononi, 2001).

In addition, the principal hubs, defined as the 10% of regions (nodes) with the highest degree for each subject, were also calculated.

Association with abnormal neurodevelopment at two years of age

Regional connectivity risk index of abnormal neurodevelopment

Due to the relatively reduced sample size, in order to avoid overfitting of the predictive models (Michel et al., 2012), a procedure to reduce the regional feature space was undertaken. Hence, in a previous step, regional connectivity features that predicted better neurodevelopment at 2-years were selected and reduced to a single index. In brief, a scheme was defined to integrate the complex process of regional brain reorganization into a single score, defined as 'regional connectivity risk index'. To this end, a leave-one-out cross validation strategy was followed to obtain a blind score integrating the relevant regional features of each IUGR infant. The scheme for the generation of this index was built according to the following steps (Fig. 2):

(1) Feature selection based on keeping those features with higher individual discriminative power of the normal/abnormal BSID-III (dicotomic value) for the training set. Specifically, those features with an absolute value two-sample *t*-test one standard deviation above the mean for the training set were selected.
(2) Computation of the nonlinear regression model that better classified the training set using the features selected in step (1) by means of a regression tree (Breiman et al., 1984).
(3) Calculation of the 'regional connectivity risk index' (probability of abnormal BSID-III) and blind classification (using a 0.5 cutoff on the probability of abnormal BSID-III) of the test sample by applying the regression tree estimated in step (2).
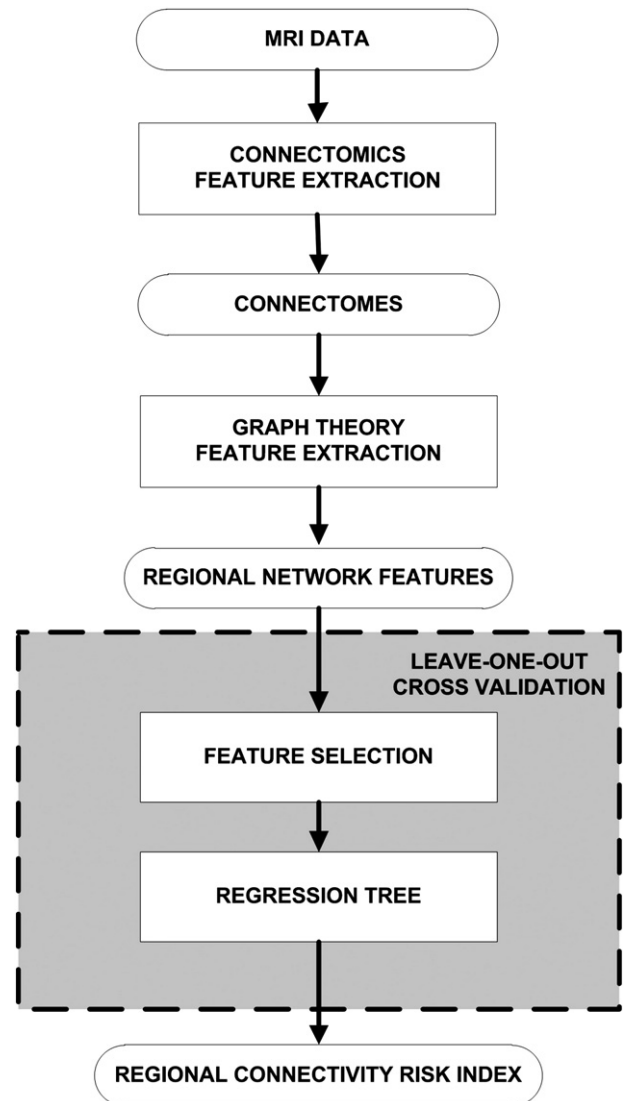
Fig. 2. Learning algorithm scheme to obtain a 'regional connectivity risk index' that integrates regional network features associated to abnormal neurodevelopment.

Subsequently, the performance of this 'regional connectivity risk index' to achieve a blind classification of the neurodevelopmental status (normal or abnormal) was evaluated.

Association of network features and clinical data to neurodevelopmental scores on BSID-III in 2 year IUGR children

Three blocks of data were established: clinical–epidemiological features (gender, smoking status, breastfeeding, GA and weight centile at birth), global network features and the regional connectivity risk index as defined in the Regional connectivity risk index of abnormal neurodevelopment section.

In order to assess the association of the three blocks of data with neurodevelopmental scores in IUGR, a binomial logistic regression with two different approaches was then conducted. In the first approach the independent association power of each block binomial logistic regression was evaluated based on an enter method. In the second approach, the three blocks were consecutively entered as predictors into a binomial logistic regression with a backward step-wise selection criterion in order to assess the best predictive model for BSID-III abnormal performance. Removal testing in backward step-wise selection was based on the probability of the likelihood-ratio statistic based on the maximum partial likelihood estimates. p value for variable removal was set at 0.15.

Statistical analysis

Statistical comparisons among groups were performed by general linear models with gender, maternal education level, smoking during pregnancy and breastfeeding as cofactors and GA as a covariate. Due to the exploratory nature of these analyses, significance was declared at $p < 0.05$ (uncorrected). In addition, the results of each regional feature were corrected for multiple comparisons with a False Discovery Rate (FDR) approach (Benjamini et al., 2006) in order to control alpha error to 5%. The software package SPSS 18.0 (SPSS, Chicago, IL) was used for the statistical analyses. All computational algorithms were implemented using MATLAB (2007b, The MathWorks Inc., Natick, MA).

Results

Basic clinical features in the study population

Structural MRI evaluation revealed the presence of anomalies in 8 IUGR (two increased cisterna magna, four ventricular dilatations and two WM lesions) and in 5 controls (two increased cisterna magna and three ventricular dilatations) that were excluded from the final analysis. In addition, 4 controls and 10 IUGR did not pass quality criteria concerning motion artifacts or correct tractography reconstruction that prevented performing further analysis. Thus, the final sample included 24 IUGR infants and 32 control infants.

As expected, anthropometric measurements at birth normalized for local standards were significantly lower in IUGR group (Table 2). No significant differences were found in GA at birth, gender distribution, Apgar score at 5 min, umbilical artery pH and rate of neonatal

Table 2
Neonatal data, demographic characteristics, growth parameters, and BSID-III scores in the study groups. Mean ($\pm$ SD). Variables with $p < 0.05$ are highlighted in bold.

	Controls n = 32	IUGR n = 24	p[a]
Neonatal data			
GA at delivery	34.8 (5.8)	36.6 (3.1)	0.173
Birth weight centile	54 (23.9)	5.5 (5.5)	**<0.001**
Length at birth centile	59.1 (23.3)	11.6 (11.8)	**<0.001**
Cephalic perimeter at birth centile	43.5 (25.1)	13.2 (17.2)	**<0.001**
Gender distribution (male/female)	17/15	15/9	0.483
Apgar 5 min	9 (2.5)	9.5 (1.7)	0.395
Umbilical artery pH	7.27 (0.07)	7.24 (0.09)	0.122
Neonatal complications	3.1% [1/32]	4.2% [1/24]	0.835
Demographic characteristics			
Maternal age [years]	31.3 (4.1)	32.2 (4.0)	0.426
Maternal education less than high school	25.8%	33.3%	0.542
Breastfeeding longer than 4 months	67.7%	59.1%	0.518
Smoking during pregnancy	12.5%	45.8%	**0.005**
Corrected age at MR [months]	12.8 (1.5)	13.2 (1.6)	0.382
Corrected age at BSID-III [months]	20.2 (3.5)	21.7 (3.0)	0.155
Growth parameters at 12 months			
Weight z-score	−0.52 (0.82)	−1.06 (0.85)	**0.024**
Height z-score	−0.17 (1.17)	−1.01 (0.97)	**0.008**
Body mass index (BMI) z-score	−0.49 (1.05)	−0.52 (0.91)	0.079
Cephalic perimeter z-score	−0.50 (1.05)	−1.09 (1.30)	0.891
BSID-III scores			
Cognitive score [b]	108.8 (12.5)	104.3 (9.4)	**0.029**[c]
Language score [b]	102.1 (19.0)	91.3 (12.5)	**0.002**[c]
Motor score [b]	106.9 (14.2)	100.7 (9.6)	**0.018**[c]
Social emotional score [d]	117.4 (30.2)	108.6 (23.7)	0.514[c]
Adaptive behavior score [d]	92.9 (17.0)	89.5 (18.8)	0.469[c]

[a] Student's *t*-test for independent samples or Pearson's Chi[2] test.
[b] Controls n = 22/IUGR n = 17.
[c] General Lineal Model significance among groups corrected for clinical covariables and cofactors.
[d] Controls n = 18/IUGR n = 16.

complications among groups. No postnatal corticosteroids were administered to any individual included in our study. Maternal smoking status during pregnancy was increased in IUGR group ($p = 0.005$). Regarding BSID-III neurodevelopmental test, IUGR infants showed a trend to worse scores than the control group in all scales, although the differences were statistically significant only for cognitive ($p = 0.029$), motor ($p = 0.018$) and language ($p = 0.002$) clusters (Table 2). Proportion of abnormal BSID-III in IUGR groups was non-significantly higher when compared with control group (47.1% vs. 27.3%, $p = 0.201$).

Small-worldness

Graph theoretical analysis on the adjacency matrices representing structural brain networks of our subjects, showed that 1-year old children structural brain networks are a small-world network of neural tracts. The comparison among local and global efficiencies of the structural brain networks and its random and lattice equivalents showed that all our population fulfilled a small-world criterion, having an intermediate global and local efficiency compared to its random and regular equivalent networks (Table 3). Using classical small-world criteria, a small-world behavior was also observed (Supplementary Table 1).

Hubs of IUGR and controls, defined as the 10% of nodes with higher degree, were identified for each group separately (Table 4). Similar hubs on both groups were found, mainly precuneus and cerebellum of each hemisphere.

Global connectivity characteristics

The analyses of unthresholded networks show that general linear models of average degree, binary global efficiency and binary local efficiency did not show statistically significantly differences between cases and controls (Figs. 3A–C). FN-weighted global and local efficiency were not significantly different in cases and controls, but there was a trend of reduced values in IUGR (Figs. 3D and E). FA-weighted global efficiency was significantly decreased in IUGR (group effect: $F = 7.15$ $p = 0.012$, Fig. 3F). FA-weighted local efficiency was also significantly lower in the IUGR group (group effect: $F = 5.99$ $p = 0.020$, Fig. 3G). Further analyses with fiber threshold from 1 to 5 are included in Supplementary Table 2.

Disrupted regional connectivity

Analysis of regional connectivity revealed statistically significant differences in IUGR at multiple levels on the set of features evaluated (Table 5, Fig. 4). For instance, differences in nodal degree were mainly observed in parietal and occipital lobe whereas all regions in temporal lobe and cerebellum demonstrated differences in betweenness centrality. Binary nodal efficiency showed most of the differences in temporal and parietal lobe and cerebellum while frontal lobe and subcortical gray nuclei were the most affected in FN-weighted nodal efficiency. Finally, FA-weighted nodal efficiency presented significant differences in multiple regions of frontal lobe and sub-cortical gray matter, almost all regions included in parietal and occipital lobe and in whole cerebellum and central region.

Association with abnormal neurodevelopment at two years of age

Regional connectivity risk index of abnormal neurodevelopment

Most discriminant regional connectivity features are shown in Fig. 5 and Supplementary Table 3. Specifically, features selected in more than 90% of leave-one-out iterations included characteristics of frontal regions (right and left precentral gyrus, left superior frontal gyrus, left superior and middle frontal gyrus orbital part, left superior frontal gyrus medial orbital part, right inferior frontal gyrus triangular

Table 3
Controls, IUGR and their equivalent random and lattice networks binary global and local efficiency. Mean ($\pm$ SD).

Fiber threshold	Group	Random global efficiency	Global efficiency	Lattice global efficiency	Random local efficiency	Local efficiency	Lattice local efficiency
1	Controls	0.8191 (0.0178)	0.8191 (0.0181)	0.8191 (0.0178)	0.8598 (0.0148)	0.8766 (0.0098)	0.8978 (0.0053)
	IUGR	0.8178 (0.0147)	0.8178 (0.0151)	0.8177 (0.0148)	0.8610 (0.0128)	0.8766 (0.0089)	0.8984 (0.0048)
2	Controls	0.7629 (0.0159)	0.7626 (0.0162)	0.7624 (0.0161)	0.8155 (0.0143)	0.8501 (0.0071)	0.8835 (0.0040)
	IUGR	0.7595 (0.0141)	0.7592 (0.0145)	0.7589 (0.0142)	0.8154 (0.0135)	0.8499 (0.0082)	0.8838 (0.0037)
3	Controls	0.7301 (0.0137)	0.7290 (0.0145)	0.7285 (0.0142)	0.7862 (0.0142)	0.8355 (0.0065)	0.8766 (0.0041)
	IUGR	0.7263 (0.0140)	0.7253 (0.0145)	0.7247 (0.0143)	0.7849 (0.0135)	0.8358 (0.0070)	0.8762 (0.0038)
4	Controls	0.7072 (0.0122)	0.7055 (0.0132)	0.7042 (0.0134)	0.7637 (0.0142)	0.8255 (0.0061)	0.8708 (0.0042)
	IUGR	0.7041 (0.0128)	0.7023 (0.0134)	0.7008 (0.0133)	0.7664 (0.0125)	0.8272 (0.0069)	0.8715 (0.0037)
5	Controls	0.6899 (0.0111)	0.6872 (0.0123)	0.6849 (0.0126)	0.7460 (0.0138)	0.8179 (0.0063)	0.8660 (0.0055)
	IUGR	0.6869 (0.0127)	0.6841 (0.0135)	0.6818 (0.0139)	0.7462 (0.0145)	0.8201 (0.0073)	0.8659 (0.0055)

part, right gyrus rectus right supplementary motor area), occipital regions (right middle occipital gyrus, left inferior occipital gyrus, left calcarine fissure and surrounding cortex) and subcortical gray matter (right and left caudate, right putamen and thalamus).

The regional connectivity risk index obtained blindly for each subject in the leave-one-out learning algorithm also allowed us to

Table 4
Principal hubs in controls and IUGR and its frequency (%) of selection at different fiber thresholds.

Fiber threshold	Controls hubs	Frequency (%)	IUGR hubs	Frequency (%)
1	PQ (L)	93.8	PQ (L)	87.5
	PQ (R)	84.4	PQ (R)	79.2
	CER (L)	84.4	CER (L)	75.0
	CER (R)	71.9	CER (R)	75.0
	CAU (L)	53.1	P1 (R)	50.0
	P1 (R)	46.9	F2 (R)	45.8
	CAU (R)	34.4	CAU (L)	41.7
	AG (R)	31.3	F2 (L)	37.5
	THA (L)	21.9	CAU (R)	33.3
2	PQ (L)	90.6	PQ (L)	87.5
	PQ (R)	84.4	PQ (R)	87.5
	CER (L)	84.4	CER (L)	83.3
	CER (R)	65.6	CER (R)	75.0
	CAU (L)	56.3	CAU (R)	54.2
	CAU (R)	43.8	P1 (R)	45.8
	P1 (R)	34.4	F2 (R)	41.7
	T1P (L)	31.3	CAU (L)	41.7
	F2 (L)	28.1	F2 (L)	33.3
3	PQ (L)	93.8	PQ (R)	91.7
	CER (L)	87.5	PQ (L)	87.5
	PQ (R)	84.4	CER (L)	75.0
	CER (R)	68.8	CER (R)	66.7
	CAU (R)	53.1	F2 (L)	58.3
	CAU (L)	50.0	CAU (R)	54.2
	F2 (L)	28.1	F2 (R)	50.0
	O2 (R)	28.1	CAU (L)	41.7
	AG (R)	28.1	F1 (R)	33.3
4	PQ (L)	87.5	PQ (L)	91.7
	PQ (R)	87.5	PQ (R)	91.7
	CER (L)	84.4	CER (L)	70.8
	CER (R)	68.8	CER (R)	70.8
	CAU (R)	53.1	F2 (R)	58.3
	CAU (L)	50.0	CAU (R)	54.2
	F2 (R)	31.3	F2 (L)	41.7
	P1 (R)	28.1	CAU (L)	41.7
	T2 (R)	28.1	T2 (R)	41.7
5	PQ (L)	90.7	PQ (L)	91.7
	PQ (R)	87.5	PQ (R)	79.2
	CER (L)	84.4	CER (L)	75.0
	CER (R)	75.0	CER (R)	75.0
	CAU (R)	53.1	F2 (R)	58.3
	CAU (L)	50.0	F2 (L)	54.2
	F2 (R)	31.3	CAU (R)	41.7
	F2 (L)	28.1	T2 (R)	41.7
	P1 (R)	28.1	F1 (R)	33.3

(L) refers to left hemisphere and (R) to right hemisphere.

blindly classify each IUGR subject into normal or abnormal BSID-III performance with an accuracy of 82.4%, with a sensitivity of 87.5% and a specificity of 77.8%.

Predictive model including clinical and MRI data

Binomial logistic regression was used to assess the predictive value of clinical data, global connectivity features and regional connectivity risk index with abnormal BSID-III performance in IUGR group (Table 6). The regression model based on clinical information (weight centile, GA, gender, maternal education level, mother smoking status during pregnancy and breastfeeding) was not significantly associated with abnormal neurodevelopment. The binomial logistic regression with global connectivity features (average degree and binary, FN-weighted and FA-weighted global and local efficiency) showed an accuracy of 76.5%, with a sensitivity of 87.5% and a specificity of 66.7%. The model had a Chi-square = 9.81 with p = 0.199 and a Nagelkerke R^2 of 0.59. None of the global connectivity features had a significant contribution by itself. Finally, previously calculated regional connectivity risk index achieved an accuracy of 82.4%, with 87.5% of sensitivity and 77.8% of specificity. The regression model was significant with a Chi-square = 7.17, p = 0.007 and a Nagelkerke R^2 of 0.46.

In an exploratory analysis, in order to find the best performing combination of predictive variables, binary logistic regression with a backwards stepwise method was applied, entering the data in three consecutive blocks: clinical–epidemiological features, global connectivity and regional connectivity risk index (Table 7). In the first block, all clinical data were discarded by the step-wise process. Entering global connectivity data in the second block leaded to a six step process in which only average degree and binary global efficiency remained. However, the model was not significant. When regional connectivity risk index was added in a third block, accuracy of the classification increased to 88.2% (sensitivity 87.5, specificity 88.9%) with a significant model (Chi-square = 11.38, p = 0.010, Nagelkerke R^2 = 0.65).

Discussion

This study describes the use of diffusion MRI based connectomics in one-year-old infants, with particular focus on the analysis of structural brain networks. The study provides evidence that diffusion MRI based connectomics can demonstrate large-scale brain reorganization of the structural brain network in one year old children who suffered IUGR by means of global as well as regional brain network feature analysis. Finally, it was demonstrated that structural brain network features evaluated at one year could predict later neurodevelopment in 2-year old children.

Small-worldness of structural brain networks

Overall, graph theory characterization showed the small-worldness of one year old brain networks based on diffusion MRI structural connectivity. These findings are in accordance with recent studies on structural brain networks based on diffusion MRI on adults (Gong et al.,
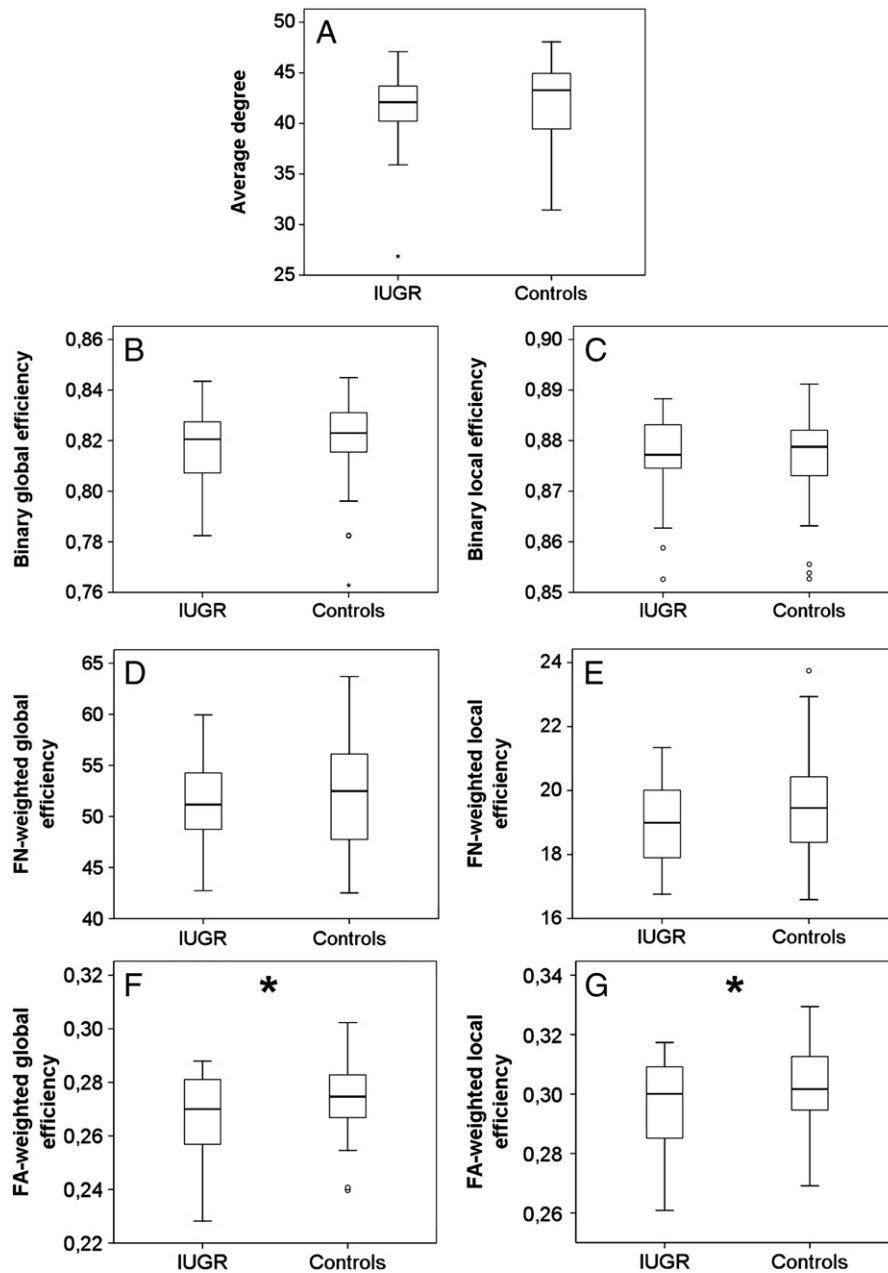
Fig. 3. Global characteristics of control and IUGR groups. (A) Average degree, (B) binary global efficiency, (C) binary local efficiency, (D) FN-weighted global efficiency, (E), FN-weighted local efficiency, (F) FA-weighted global efficiency and (G) FA-weighted local efficiency. *p<0.05.

2009; Hagmann et al., 2008), late developing brain (Hagmann et al., 2010) and brain networks based on regional volumes correlations in early developing brain (Fan et al., 2011). The results are indicative of a high connectivity organization and efficiency already at one year of age. Random networks communicate every pair of nodes with relatively few intermediate steps, but have a lack of organization. On the contrary, lattice networks have a high level of organization but a poor average capability to efficiently communicate a given pair of nodes. Small-world networks present a balance between both kinds of networks (Sporns and Tononi, 2001) and have been reported in a wide range of networks present in nature as well as in man-made systems (Bullmore and Sporns, 2009).

Interestingly, we identified precuneus as one of the principal hubs in our one-year-old population, which is in line with previously reported results in infants (Yap et al., 2011) and in adults (Gong et al., 2009; Hagmann et al., 2008; Tomasi and Volkow, 2011).

Global structural brain network features

There is increasing agreement that network features indicate differences in brain organization (Bassett and Bullmore, 2009). Consequently, global brain network features may be a useful approach to identify which kind and at which level of complexity brain reorganization occurs. By means of weighted measures of efficiency, alterations in global and local efficiency were observed. These findings might suggest brain reorganization of the WM connectivity without significant changes in the total amount of connections. The results suggest that FA-weighted approach could be a more sensitive parameter to reveal brain reorganization due to IUGR. This is in line with previous studies suggesting the value of weighted metrics of brain networks to assess subtle differences in neurodegenerative and psychiatric conditions (Lo et al., 2010; Shu et al., 2011; Wang et al., 2012; Wee et al., 2010). In addition, weighted measures seem to correlate better with intelligence

measured by IQ score in normal subjects (Li et al., 2009). Lower global efficiency has been described in multiple sclerosis (Shu et al., 2011), schizophrenia (Wang et al., 2012), Alzheimer's disease (Lo et al., 2010) and early blindness (Shu et al., 2009). A few studies have evaluated global efficiency in relation with normal neurodevelopment. A pattern of increasing values with increasing age from 2 to 18 years of age has been described (Hagmann et al., 2010), while similar global efficiency values were measured in neonates, one-year-old and two-year-old infants (Yap et al., 2011).

FA-weighted local efficiency was also significantly lower in the IUGR group. The clinical implications of local efficiency are still undefined. While some have reported decreased local efficiency in schizophrenia (Alexander-Bloch et al., 2010; Wang et al., 2010), multiple sclerosis (He et al., 2009b; Shu et al., 2011) and children with severe reading difficulties (Vourkas et al., 2010), others found increased local efficiency in attention deficit hyperactivity disorder (Wang et al., 2009). Late developing brains (2–18 years) show decreasing clustering coefficients, and hence decreasing local efficiency, with increasing age (Hagmann et al., 2010). An increase in diffusion MRI local efficiency values has been observed during the first years of life (Yap et al., 2011).

Regional structural brain network features

Analysis of regional brain network features allowed extracting information of the topological changes on each region and its associated network. Regional characteristics were altered following a diffuse pattern along the whole brain, which included multiple areas as frontal, temporal, parietal and occipital lobes, subcortical GM nuclei, insular cortex and cerebellum. Frontal and temporal areas showed changes in all regional features, although alterations in frontal areas were found mainly in FN-weighted nodal efficiency. Frontal and temporal areas are involved in the regulation of functions previously reported to be abnormal in IUGR children, including short-term memory (Geva et al., 2006a), learning abilities (Geva et al., 2006b), attention (Heinonen et al., 2010) and social skills (Eixarch et al., 2008). Fronto-temporal areas have also been related with attention deficit hyperactivity disorder (Kobel et al., 2010), which is present in higher proportion in children who suffered IUGR (Heinonen et al., 2010). Parietal areas showed differences mainly in nodal degree and FA-weighted nodal efficiency. These findings are consistent with the poorer performance in BSID-III motor domain observed in IUGR children. Previous studies have linked worst motor performance with reduced GM in parietal areas of IUGR (Padilla et al., 2011). Occipital areas were altered mainly on FA-weighted nodal efficiency, but also on nodal degree in a less spread pattern. This result is consistent with previous findings where parieto-occipital and inferior occipital regional vulnerability to IUGR has been demonstrated (Thompson et al., 2007). Some subcortical GM nuclei including amygdala, putamen, pallidum and thalamus were also found altered, by regional features, mainly by FN-weighted nodal efficiency. Interestingly, striatal injury has been related to perinatal disorders, including IUGR, suggesting that it could be a risk factor of behavioral disturbances (Toft, 1999) and specific alterations in the cortico-striato-thalamic network have been associated with cognitive disorders, including Tourette syndrome (Makki et al., 2009), bipolar disorder (Chen et al., 2006) and attention deficit hyperactivity disorder (Castellanos et al., 1994; Faraone and Biederman, 1998). Finally, cerebellum alterations in nodal degree and weighted nodal efficiency were found. These findings are in line with previously described decreases in cerebellar WM in IUGR infants (Padilla et al., 2011) and with alterations in cerebellar neuron population in animal models of IUGR (Mallard et al., 2000).

Association with abnormal neurodevelopment at two years of age

In this study IUGR infants showed significantly worse performance in cognitive, motor and language scores on the BSID-III areas. These findings are in line with previous data in IUGR infants and

children (Bassan et al., 2011; Eixarch et al., 2008; Feldman and Eidelman, 2006; Geva et al., 2006a,b; Jarvis et al., 2003; Leitner et al., 2007; Marsal, 2002; McCarton et al., 1996; Scherjon et al., 2000). The results of this study provide evidence that graph theory features of structural brain network at one year of age carry relevant individual information related with adverse neurodevelopment measured one year later by BSID-III. Specifically, we have shown that global network connectivity features were associated to abnormal neurodevelopment. Furthermore, regional connectivity features allowed to blindly classify abnormal neurodevelopment in IUGR with an accuracy of 82.4%. By means of an exploratory backward step-wise logistic regression, we also demonstrated that mean degree and binary global efficiency in combination with regional connectivity risk index, increased the association power, to 88.2%, and achieved a very high goodness of fit of the model (Nagelkerke $R^2 = 0.65$). These results are in line with previous studies relating neurofunction with diffusion MRI based structural brain network features. Thus, global efficiency has been previously demonstrated to be associated with intelligence (Li et al., 2009), and regional features of brain networks selected by means of a learning algorithm have been related successfully to mild cognitive impairment in studies attempting to develop early biomarkers for Alzheimer's disease (Wee et al., 2010). The data here reported and previous studies suggest that combining global and regional characteristics could help to improve the understanding of neurofunctional mechanisms underlying structural connectivity. In addition, further studies linking structural and functional networks would be very helpful in order to better understand the intricate link between structural and functional connectivity in the infant brain. Combined analysis of both substrates is warranted in future studies to advance in the understanding of brain reorganization and its relation with altered neurobehavior due to IUGR and other prenatal condition. Several studies have demonstrated the feasibility of the estimation of resting-state functional MRI networks in infants, and revealed some of the principal functional hubs in the developing brain (Doria et al., 2010; Fransson et al., 2007, 2010; Smyser et al., 2010, 2011). The link between functional and structural networks has been scarcely investigated. There is preliminary evidence that structural connections are predictive of functional connections (Honey et al., 2010), but specific studies in the developing brain are lacking.

Strengths and limitations of the study

One of the most noteworthy strengths of the current study is that it was performed in well-defined cohorts diagnosed prenatally and followed prospectively. While most perinatal and demographic characteristics were not significantly different among groups, the results were corrected for a substantial number of potential confounders.

Notwithstanding, some issues must be noted concerning the methodology followed. The techniques used on a series of complex analyses, and due to their relative novelty there is a lack of 'gold standards' in the literature. Brain parcellation in young infants is a controversial subject and tissue segmentation in infant brains is considered a challenging task due to the isointense developmental pattern which results in a poor differentiation between GM and WM (Paus et al., 2001). To minimize this limitation we used high quality T1 weighted 3-Tesla Magnetic Resonance images and to guide the segmentation we used appropriate brain tissue probability maps (Altaye et al., 2008) and a pediatric atlas (Shi et al., 2011). In addition, each scan was reviewed to determine if the results of the tissue segmentation were accurate (Knickmeyer et al., 2008). A drawback of DTI tractography reconstruction is that it is highly sensitive to motion artifacts during acquisition. This prevented us to analyze a remarkable number of subjects. It is also well known that DTI is not able to encode multi-directional diffusion information, which may lead to errors in regions with a high amount of crossing fibers. Other techniques such as Q-Ball Imaging (QBI) (Tuch, 2004) or Diffusion Spectrum Imaging (DSI) (Wedeen et al., 2005) should be

Table 5
Regions with statistically significant differences in nodal degree, betweenness centrality, binary nodal efficiency, FN-weighted nodal efficiency and FA-weighted nodal efficiency in IUGR compared with controls.

ROI	Nodal degree	Betweenness centrality	Binary nodal efficiency	FN-weighted nodal efficiency	FA-weighted nodal efficiency
PRE (L)	N.S.	N.S.	N.S.	N.S.	**p = 0.025** **F = 5.507**
PRE (R)	N.S.	N.S.	N.S.	N.S.	**p = 0.027** **F = 5.393**
F1 (L)	N.S.	N.S.	N.S.	N.S.	N.S.
F1 (R)	N.S.	N.S.	N.S.	N.S.	N.S.
F1O (L)	N.S.	N.S.	N.S.	N.S.	N.S.
F1O (R)	N.S.	N.S.	N.S.	N.S.	N.S.
F2 (L)	N.S.	N.S.	N.S.	p = 0.023 F = 5.650	**p = 0.032** **F = 5.024**
F2 (R)	N.S.	N.S.	N.S.	N.S.	N.S.
F2O (L)	N.S.	N.S.	N.S.	p = 0.023 F = 5.721	N.S.
F2O (R)	N.S.	N.S.	N.S.	p = 0.009 F = 7.603	N.S.
F3OP (L)	N.S.	N.S.	N.S.	N.S.	**p = 0.021** **F = 5.870**
F3OP (R)	N.S.	N.S.	N.S.	N.S.	N.S.
F3T (L)	N.S.	N.S.	N.S.	N.S.	N.S.
F3T (R)	N.S.	N.S.	N.S.	p = 0.013 F = 6.922	N.S.
F3O (L)	p = 0.012 F = 7.133	p = 0.006 F = 8.578	p = 0.020 F = 5.930	p = 0.019 F = 6.097	N.S.
F3O (R)	N.S.	N.S.	N.S.	N.S.	N.S.
RO (L)	N.S.	N.S.	N.S.	N.S.	p = 0.035 F = 4.814
RO (R)	N.S.	N.S.	N.S.	N.S.	p = 0.038 F = 4.667
SMA (L)	N.S.	N.S.	N.S.	N.S.	**p = 0.027** **F = 5.377**
SMA (R)	N.S.	N.S.	N.S.	p = 0.033 F = 4.977	N.S.
OC (L)	N.S.	N.S.	N.S.	N.S.	N.S.
OC (R)	N.S.	N.S.	N.S.	**p = 0.003** **F = 10.618**	N.S.
F1M (L)	N.S.	N.S.	N.S.	N.S.	**p = 0.021** **F = 5.895**
F1M (R)	N.S.	N.S.	N.S.	N.S.	N.S.
F1MO (L)	N.S.	N.S.	N.S.	N.S.	N.S.
F1MO (R)	N.S.	N.S.	N.S.	N.S.	N.S.
GR (L)	N.S.	N.S.	N.S.	N.S.	N.S.
GR (R)	N.S.	N.S.	N.S.	N.S.	N.S.
IN (L)	N.S.	N.S.	N.S.	N.S.	N.S.
IN (R)	N.S.	N.S.	N.S.	N.S.	N.S.
ACIN (L)	N.S.	N.S.	N.S.	N.S.	N.S.
ACIN (R)	N.S.	N.S.	N.S.	N.S.	N.S.
MCIN (L)	N.S.	N.S.	N.S.	p = 0.020 F = 6.020	N.S.
MCIN (R)	N.S.	p = 0.010 F = 7.387	p = 0.023 F = 5.679	N.S.	p = 0.037 F = 4.742
PCIN (L)	N.S.	N.S.	N.S.	N.S.	N.S.
PCIN (R)	N.S.	N.S.	N.S.	N.S.	N.S.
HIP (L)	N.S.	N.S.	N.S.	N.S.	N.S.
HIP (R)	N.S.	N.S.	N.S.	N.S.	N.S.
PHIP (L)	N.S.	N.S.	N.S.	N.S.	N.S.
PHIP (R)	N.S.	N.S.	N.S.	N.S.	N.S.
AMYG (L)	N.S.	N.S.	N.S.	N.S.	p = 0.035 F = 4.839
AMYG (R)	N.S.	N.S.	N.S.	N.S.	N.S.
V1 (L)	N.S.	N.S.	N.S.	N.S.	**p = 0.003** **F = 10.644**
V1 (R)	N.S.	N.S.	N.S.	N.S.	**p = 0.005** **F = 8.950**
Q (L)	N.S.	N.S.	N.S.	N.S.	**p = 0.001** **F = 14.081**
Q (R)	N.S.	N.S.	N.S.	N.S.	**p = 0.013** **F = 6.975**
LING (L)	N.S.	N.S.	N.S.	N.S.	**p = 0.003** **F = 10.601**
LING (R)	N.S.	N.S.	N.S.	p = 0.024 F = 5.562	**p = 0.008** **F = 7.843**
O1 (L)	N.S.	N.S.	N.S.	N.S.	**p = 0.005** **F = 8.999**

Table 5 (continued)

ROI	Nodal degree	Betweenness centrality	Binary nodal efficiency	FN-weighted nodal efficiency	FA-weighted nodal efficiency
O1 (R)	p = 0.035 F = 4.830	N.S.	N.S.	N.S.	**p = 0.005** **F = 9.038**
O2 (L)	p = 0.039 F = 4.634	N.S.	N.S.	N.S.	**p = 0.010** **F = 7.395**
O2 (R)	p = 0.028 F = 5.319	N.S.	N.S.	N.S.	**p < 0.001** **F = 16.938**
O3 (L)	N.S.	N.S.	N.S.	N.S.	**p = 0.007** **F = 8.289**
O3 (R)	N.S.	N.S.	N.S.	N.S.	**p = 0.004** **F = 9.551**
FUSI (L)	N.S.	N.S.	N.S.	N.S.	**p = 0.008** **F = 8.105**
FUSI (R)	N.S.	N.S.	N.S.	N.S.	N.S.
POST (L)	p = 0.006 F = 8.499	N.S.	N.S.	N.S.	**p = 0.008** **F = 7.948**
POST (R)	N.S.	p = 0.015 F = 6.540	p = 0.043 F = 4.437	N.S.	**p = 0.007** **F = 8.340**
P1 (L)	**p < 0.001** **F = 15.774**	N.S.	N.S.	N.S.	**p = 0.003** **F = 10.659**
P1 (R)	N.S.	N.S.	N.S.	N.S.	**p = 0.004** **F = 9.322**
P2 (L)	p = 0.022 F = 5.736	N.S.	N.S.	N.S.	**p = 0.003** **F = 10.711**
P2 (R)	N.S.	N.S.	N.S.	N.S.	**p = 0.006** **F = 8.515**
SMG (L)	N.S.	N.S.	N.S.	N.S.	**p = 0.008** **F = 7.866**
SMG (R)	N.S.	p = 0.009 F = 7.757	p = 0.012 F = 7.064	N.S.	N.S.
AG (L)	p = 0.017 F = 6.288	N.S.	N.S.	N.S.	**p = 0.007** **F = 8.395**
AG (R)	p = 0.046 F = 4.301	N.S.	N.S.	p = 0.012 F = 7.128	**p = 0.006** **F = 8.560**
PQ (L)	N.S.	p = 0.046 F = 4.307	p = 0.016 F = 6.513	N.S.	**p = 0.005** **F = 9.156**
PQ (R)	N.S.	N.S.	N.S.	N.S.	**p = 0.012** **F = 7.040**
PCL (L)	N.S.	N.S.	N.S.	N.S.	**p = 0.012** **F = 7.040**
PCL (R)	N.S.	N.S.	p = 0.025 F = 5.542	N.S.	N.S.
CAU (L)	N.S.	N.S.	N.S.	N.S.	N.S.
CAU (R)	N.S.	N.S.	N.S.	N.S.	N.S.
PUT (L)	N.S.	N.S.	N.S.	p = 0.043 F = 4.445	p = 0.036 F = 4.799
PUT (R)	N.S.	N.S.	N.S.	**p = 0.001** **F = 13.440**	N.S.
PAL (L)	N.S.	N.S.	N.S.	p = 0.025 F = 5.556	N.S.
PAL (R)	N.S.	N.S.	N.S.	p = 0.014 F = 6.738	N.S.
THA (L)	N.S.	N.S.	N.S.	N.S.	N.S.
THA (R)	N.S.	N.S.	N.S.	p = 0.035 F = 4.814	**p = 0.016** **F = 6.449**
HES (L)	N.S.	N.S.	N.S.	N.S.	**p = 0.028** **F = 5.271**
HES (R)	N.S.	p = 0.031 F = 5.061	p = 0.012 F = 7.131	N.S.	p = 0.041 F = 4.506
T1 (L)	N.S.	p = 0.037 F = 4.710	p = 0.011 F = 7.235	N.S.	**p = 0.016** **F = 6.432**
T1 (R)	N.S.	**p < 0.001** **F = 17.798**	p = 0.001 F = 14.411	N.S.	N.S.
T1P (L)	N.S.	N.S.	N.S.	**p = 0.002** **F = 11.304**	N.S.
T1P (R)	N.S.	N.S.	N.S.	p = 0.029 F = 5.225	N.S.
T2 (L)	p = 0.028 F = 5.305	p = 0.005 F = 9.172	p = 0.005 F = 9.263	N.S.	**p = 0.024** **F = 5.616**
T2 (R)	N.S.	**p < 0.001** **F = 15.620**	p = 0.001 F = 12.612	N.S.	**p = 0.010** **F = 7.516**
T2P (L)	p = 0.046 F = 4.285	p = 0.042 F = 4.468	N.S.	p = 0.027 F = 5.332	N.S.
T2P (R)	N.S.	N.S.	N.S.	N.S.	N.S.
T3 (L)	N.S.	p = 0.038 F = 4.647	p = 0.006 F = 8.652	N.S.	**p = 0.004** **F = 9.339**
T3 (R)	N.S.	N.S.	N.S.	N.S.	

Table 5 (*continued*)

ROI	Nodal degree	Betweenness centrality	Binary nodal efficiency	FN-weighted nodal efficiency	FA-weighted nodal efficiency
					p = 0.017 **F = 6.273**
CER (L)	p = 0.023 F = 5.657	N.S.	N.S.	**p < 0.001** **F = 15.467**	**p = 0.011** **F = 7.346**
CER (R)	p = 0.042 F = 4.471	N.S.	N.S.	**p < 0.001** **F = 19.769**	**p = 0.003** **F = 10.630**
VER	p = 0.026 F = 5.453	N.S.	N.S.	p = 0.006 F = 8.539	**p = 0.016** **F = 6.467**

Features that maintain significance after False Discovery Rate controlling alpha error to 0.05 are highlighted in bold. (L) refers to left hemisphere, (R) to right hemisphere. N.S. for Not Significant.

used to solve this issue and provide more accurate WM tractography reconstruction in future studies. Current limitations of DTI based tractography, and the noisy nature of the acquisitions, may result in the inclusion of spurious connections in individual networks. However, it must be noted that we did not perform an analysis directly based on edges, but measured network topology features. This approach is robust against noise as it integrates overall information of the individual networks, and therefore, minimizes the effect of spurious connections. How the connectivity between regions must be quantified is also an issue to be addressed. Binarization of the obtained network implies a loss of information of the connectivity pattern, and some authors propose different measures to quantify connections based on diffusion MRI as the number of fiber bundles, density of fibers or average measures of diffusion along the tract (Hagmann et al., 2007; Li et al., 2009; Wee et al., 2010). However, how the weight of a connection must be quantified, and its correlation with the anatomical substrate in which transfer of neural signals yields is still an open question (Li et al., 2009; Shu et al., 2009). It must be noted that average degree, and therefore the network cost, were non-significantly different between groups in the unthresholded networks, which supports that similar network density of WM connections were calculated throughout all the population, minimizing the chances of differences in network cost causing some of the observed differences.

It is also worth noticing that the proportion of control subjects with abnormal Bayley scores may seem relatively high (27%). Part of the control population was composed by prematurely born infants, which by definition are associated with increased rates of neurodevelopmental delay (Darlow et al., 2009). While we cannot exclude that this may have hampered the demonstration of some differences, correction for prematurity was important to ensure that differences are most likely the consequence of intrauterine growth restriction. Finally, we acknowledge that the relatively reduced sample size used in the present study prevents to generalize the set of altered features that predict an abnormal BSID-III performance. Larger sample sizes will help to estimate the generality of the identified regions in future studies and the robustness of the learning algorithm.

Conclusion

In conclusion, MRI connectomics is an emerging technique that is suitable for the assessment of brain reorganization in IUGR infants by means of global and regional graph theory based network features,
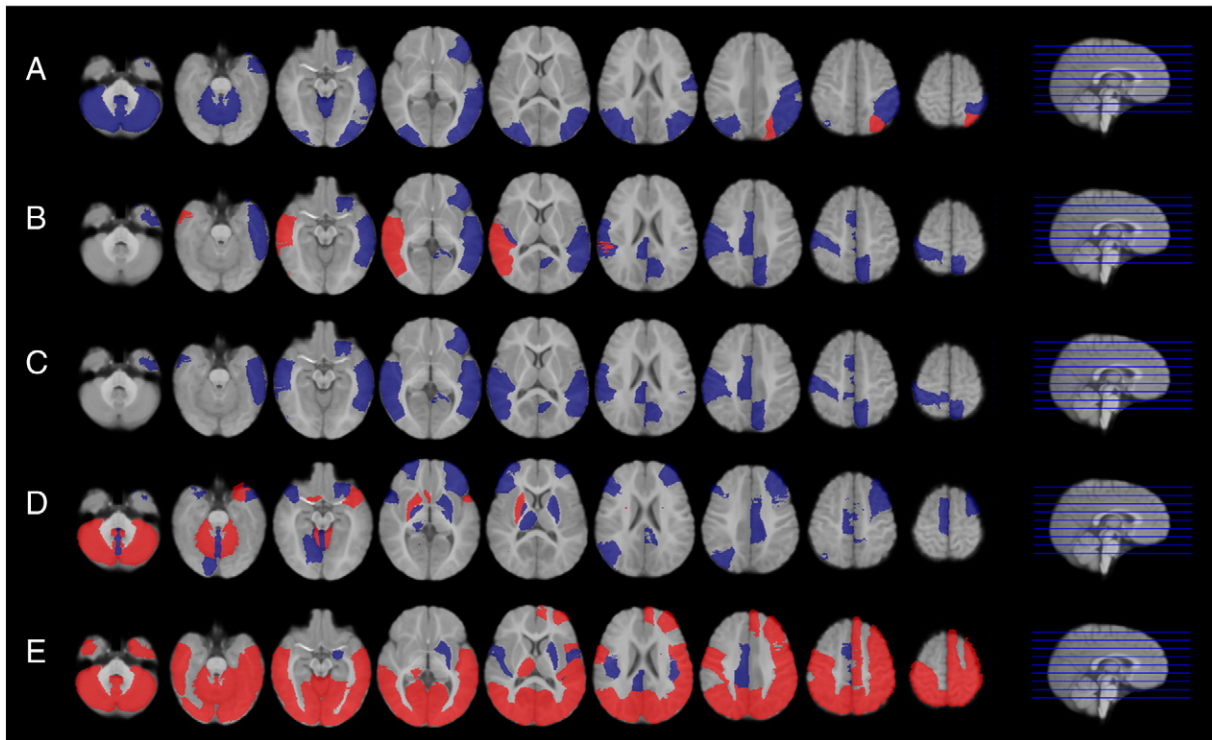
Fig. 4. Altered regional features in IUGR. In blue, regional characteristics showing statistically significant differences (p<0.05) in IUGR. In red, those regional characteristics that remained statistically significant after False Discovery Rate controlling alpha error at 5%. (A) Nodal degree, (B) betweenness centrality, (C) binary nodal efficiency, (D) FN-weighted nodal efficiency and (E) FA-weighted nodal efficiency. (For interpretation of the references to color in this figure legend, the reader is referred to the web version of this article.)
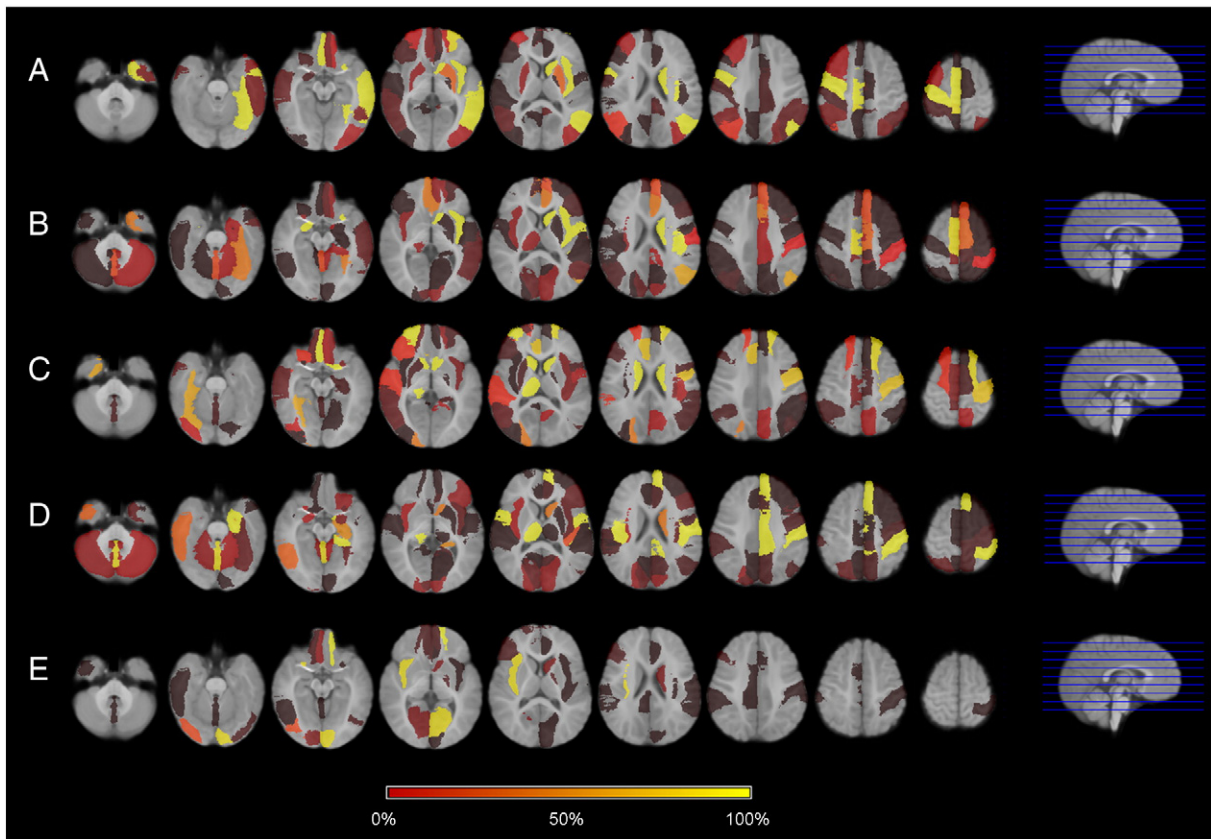
Fig. 5. Regional features associated with an abnormal BSID-III outcome in IUGR expressed as the frequency (%) of selection in the leave-one-out algorithm. (A) Nodal degree, (B) betweenness centrality, (C) binary nodal efficiency, (D) FN-weighted nodal efficiency and (E) FA-weighted nodal efficiency.

which are related to different levels of organizational complexity. We could demonstrate altered brain network topology in one-year-old IUGR infants and its association with abnormal performance in neurodevelopmental scales (BSID-III) at two years of age. Larger studies

are required to validate the results here reported. However, the findings show the potential of diffusion MRI based connectomics and graph theory based network analysis for extracting features that characterize the individual architecture of neural circuitry. Hence, this methodology holds as a promising candidate for the

Table 6
Binomial logistic regression (enter method) of abnormal Bayleys performance using three blocks of predictors: clinical characteristics, global connectivity features, and regional connectivity risk index.

	B	S.E.	Wald	df	Sig.
Clinical characteristics					
(Cox and Snell R^2: 0.155; Nagelkerke R^2: 0.207; model significance: p = 0.825)					
Maternal education	−0.610	1.646	0.137	1	0.711
Smoking status	0.791	1.292	0.375	1	0.540
Gender	0.404	1.238	0.106	1	0.744
Breastfeeding more than 4 months	1.081	1.394	0.602	1	0.438
GA	−0.135	0.246	0.300	1	0.584
Weight centile	−0.021	0.300	0.005	1	0.945
Constant	3.953	9.952	0.158	1	0.691
Global connectivity features					
(Cox and Snell R^2: 0.439; Nagelkerke R^2: 0.585; model significance: p = 0.199)					
Mean degree	1.601	1.452	1.216	1	0.270
Binary global efficiency	−491.020	672.818	0.533	1	0.466
Binary local efficiency	274.691	621.901	0.195	1	0.659
FN-weighted global efficiency	0.894	1.016	0.775	1	0.379
FN-weighted local efficiency	−4.375	4.024	1.182	1	0.277
FA-weighted global efficiency	−537.727	1046.374	0.264	1	0.607
FA-weighted local efficiency	688.091	1061.576	0.420	1	0.517
Constant	68.287	124.702	0.300	1	0.584
Regional connectivity features					
(Cox and Snell R^2: 0.344; Nagelkerke R^2: 0.459; model significance: p = 0.007)					
Regional connectivity risk index	3.348	1.443	5.384	1	0.020
Constant	−1.805	1.014	3.170	1	0.075

Table 7
Binomial logistic regression (step-wise backward method) of abnormal Bayleys performance in three consecutive blocks including clinical characteristics, global connectivity features, and regional connectivity risk index. Results are the last step of the backward algorithm.

Number of steps	Variables remaining in the step	B	S.E.	Wald	Sig. in the equation	Sig. of the model change if removed
Block1: clinical characteristics						
(Cox and Snell R^2: 0.000; Nagelkerke R^2: 0.000; model significance: p = 0.229)						
7	Constant	−0.118	0.486	0.059	0.808	–
Block2: clinical characteristics + global connectivity features						
(Cox and Snell R^2: 0.250; Nagelkerke R^2: 0.333; model significance: p = 0.087)						
6	Mean degree	0.361	0.305	1.402	0.236	0.105
	Binary global efficiency	−94.774	61.936	2.342	0.126	0.050
	Constant	62.155	41.914	2.199	0.138	–
Block3: clinical characteristics + global connectivity features + regional connectivity risk index						
(Cox and Snell R^2: 0.488; Nagelkerke R^2: 0.651; model significance: p = 0.010)						
1	Mean degree	0.757	0.527	2.069	0.150	–
	Global efficiency	−150.857	97.979	2.371	0.124	–
	Regional connectivity risk index	4.238	2.177	3.790	0.052	0.011
	Constant	89.089	61.150	2.123	0.145	–

development of imaging biomarkers of poor neurodevelopmental outcome in infants at risk due to prenatal diseases.

Acknowledgments

Appendix A. Supplementary data

Supplementary data to this article can be found online at doi:10.1016/j.neuroimage.2012.01.059.

References

Achard, S., Bullmore, E., 2007. Efficiency and cost of economical brain functional networks. PLoS Comput. Biol. 3, e17.

Alexander-Bloch, A.F., Gogtay, N., Meunier, D., Birn, R., Clasen, L., Lalonde, F., Lenroot, R., Giedd, J., Bullmore, E.T., 2010. Disrupted modularity and local connectivity of brain functional networks in childhood-onset schizophrenia. Front. Syst. Neurosci. 4, 147.

Altaye, M., Holland, S.K., Wilke, M., Gaser, C., 2008. Infant brain probability templates for MRI segmentation and normalization. NeuroImage 43, 721–730.

Anderson, P.J., De Luca, C.R., Hutchinson, E., Roberts, G., Doyle, L.W., 2010. Underestimation of developmental delay by the new Bayley-III Scale. Arch. Pediatr. Adolesc. Med. 164, 352–356.

Ashburner, J., Friston, K.J., 2005. Unified segmentation. NeuroImage 26, 839–851.

Baschat, A.A., 2004. Pathophysiology of fetal growth restriction: implications for diagnosis and surveillance. Obstet. Gynecol. Surv. 59, 617–627.

Bassan, H., Stolar, O., Geva, R., Eshel, R., Fattal-Valevski, A., Leitner, Y., Waron, M., Jaffa, A., Harel, S., 2011. Intrauterine growth-restricted neonates born at term or preterm: how different? Pediatr. Neurol. 44, 122–130.

Bassett, D.S., Bullmore, E.T., 2009. Human brain networks in health and disease. Curr. Opin. Neurol. 340–347.

Bassett, D.S., Bullmore, E., Verchinski, B.A., Mattay, V.S., Weinberger, D.R., Meyer-Lindenberg, A., 2008. Hierarchical organization of human cortical networks in health and schizophrenia. J. Neurosci. 28, 9239–9248.

Benjamini, Y., Krieger, A.M., Yekutieli, D., 2006. Adaptive linear step-up procedures that control the false discovery rate. Biometrika 93, 491–507.

Breiman, L., Friedman, J.H., Olshen, R.A., Stone, C.G., 1984. Classification and Regression Trees. CRC Press, Boca Raton, FL.

Bullmore, E., Sporns, O., 2009. Complex brain networks: graph theoretical analysis of structural and functional systems. Nat. Rev. Neurosci. 10, 186–198.

Castellanos, F.X., Giedd, J.N., Eckburg, P., Marsh, W.L., Vaituzis, A.C., Kaysen, D., Hamburger, S.D., Rapoport, J.L., 1994. Quantitative morphology of the caudate nucleus in attention deficit hyperactivity disorder. Am. J. Psychiatry 151, 1791–1796.

Chen, C.H., Lennox, B., Jacob, R., Calder, A., Lupson, V., Bisbrown-Chippendale, R., Suckling, J., Bullmore, E., 2006. Explicit and implicit facial affect recognition in manic and depressed states of bipolar disorder: a functional magnetic resonance imaging study. Biol. Psychiatry 59, 31–39.

Darlow, B.A., Horwood, L.J., Wynn-Williams, M.B., Mogridge, N., Austin, N.C., 2009. Admissions of all gestations to a regional neonatal unit versus controls: 2-year outcome. J. Paediatr. Child Health 45, 187–193.

Doria, V., Beckmann, C.F., Arichi, T., Merchant, N., Groppo, M., Turkheimer, F.E., Counsell, S.J., Murgasova, M., Aljabar, P., Nunes, R.G., Larkman, D.J., Rees, G., Edwards, A.D., 2010. Emergence of resting state networks in the preterm human brain. Proc. Natl. Acad. Sci. U. S. A. 107, 20015–20020.

Dubois, J., Benders, M., Borradori-Tolsa, C., Cachia, A., Lazeyras, F., Ha-Vinh Leuchter, R., Sizonenko, S.V., Warfield, S.K., Mangin, J.F., Hüppi, P.S., 2008. Primary cortical folding in the human newborn: an early marker of later functional development. Brain 131, 2028–2041.

Eixarch, E., Meler, E., Iraola, A., Illa, M., Crispi, F., Hernandez-Andrade, E., Gratacos, E., Figueras, F., 2008. Neurodevelopmental outcome in 2-year-old infants who were small-for-gestational age term fetuses with cerebral blood flow redistribution. Ultrasound Obstet. Gynecol. 32, 894–899.

Esteban, F.J., Padilla, N., Sanz-Cortes, M., de Miras, J.R., Bargallo, N., Villoslada, P., Gratacos, E., 2010. Fractal-dimension analysis detects cerebral changes in preterm infants with and without intrauterine growth restriction. NeuroImage 53, 1225–1232.

Fan, Y., Shi, F., Smith, J.K., Lin, W., Gilmore, J.H., Shen, D., 2011. Brain anatomical networks in early human brain development. NeuroImage 54, 1862–1871.

Faraone, S.V., Biederman, J., 1998. Neurobiology of attention-deficit hyperactivity disorder. Biol. Psychiatry 44, 951–958.

Feldman, R., Eidelman, A.I., 2006. Neonatal state organization, neuromaturation, mother–infant interaction, and cognitive development in small-for-gestational-age premature infants. Pediatrics 118, e869–e878.

Figueras, F., Meler, E., Iraola, A., Eixarch, E., Coll, O., Figueras, J., Francis, A., Gratacos, E., Gardosi, J., 2008. Customized birthweight standards for a Spanish population. Eur. J. Obstet. Gynecol. Reprod. Biol. 136, 20–24.

Figueras, F., Oros, D., Cruz-Martinez, R., Padilla, N., Hernandez-Andrade, E., Botet, F., Costas-Moragas, C., Gratacos, E., 2009. Neurobehavior in term, small-for-gestational age infants with normal placental function. Pediatrics 124, e934–e941.

Fillard, P., Pennec, X., Arsigny, V., Ayache, N., 2007. Clinical DT-MRI estimation, smoothing, and fiber tracking with log-Euclidean metrics. IEEE Trans. Med. Imaging 26, 1472–1482.

Fransson, P., Skiold, B., Horsch, S., Nordell, A., Blennow, M., Lagercrantz, H., Aden, U., 2007. Resting-state networks in the infant brain. Proc. Natl. Acad. Sci. U. S. A. 104, 15531–15536.

Fransson, P., Aden, U., Blennow, M., Lagercrantz, H., 2010. The functional architecture of the infant brain as revealed by resting-state FMRI. Cereb. Cortex 21, 145–154.

Geva, R., Eshel, R., Leitner, Y., Fattal-Valevski, A., Harel, S., 2006a. Memory functions of children born with asymmetric intrauterine growth restriction. Brain Res. 1117, 186–194.

Geva, R., Eshel, R., Leitner, Y., Valevski, A.F., Harel, S., 2006b. Neuropsychological outcome of children with intrauterine growth restriction: a 9-year prospective study. Pediatrics 118, 91–100.

Gong, G., He, Y., Concha, L., Lebel, C., Gross, D.W., Evans, A.C., Beaulieu, C., 2009. Mapping anatomical connectivity patterns of human cerebral cortex using in vivo diffusion tensor imaging tractography. Cereb. Cortex 19, 524–536.

Hagmann, P., 2005. From Diffusion MRI to Brain Connectomics. Signal Processing Institute. Ecole Polytechnique Fédérale de Lausanne (EPFL), Lausane.

Hagmann, P., Kurant, M., Gigandet, X., Thiran, P., Wedeen, V.J., Meuli, R., Thiran, J.P., 2007. Mapping human whole-brain structural networks with diffusion MRI. PLoS One 2, e597.

Hagmann, P., Cammoun, L., Gigandet, X., Meuli, R., Honey, C., Wedeen, V.J., Sporns, O., 2008. Mapping the structural core of human cerebral cortex. PLoS Biol. 6e, 159.

Hagmann, P., Sporns, O., Madan, N., Cammoun, L., Pienaar, R., Wedeen, V.J., Meuli, R., Thiran, J.P., Grant, P.E., 2010. White matter maturation reshapes structural connectivity in the late developing human brain. Proc. Natl. Acad. Sci. U. S. A. 107, 19067–19072.

Hänggi, J., Wotruba, D., Jancke, L., 2011. Globally altered structural brain network topology in grapheme-color synesthesia. J. Neurosci. 31, 5816–5828.

He, Y., Chen, Z., Evans, A.C., 2008. Structural insights into aberrant topological patterns of large-scale cortical networks in Alzheimer's disease. J. Neurosci. 28, 8148–8159.

He, Y., Chen, Z., Gong, G., Evans, A., 2009a. Neuronal networks in Alzheimer's disease. Neuroscientist 15, 333.

He, Y., Dagher, A., Chen, Z., Charil, A., Zijdenbos, A., Worsley, K., Evans, A., 2009b. Impaired small-world efficiency in structural cortical networks in multiple sclerosis associated with white matter lesion load. Brain 132, 3366–3379.

Heinonen, K., Raikkonen, K., Pesonen, A.K., Andersson, S., Kajantie, E., Eriksson, J.G., Wolke, D., Lano, A., 2010. Behavioural symptoms of attention deficit/hyperactivity disorder in preterm and term children born small and appropriate for gestational age: a longitudinal study. BMC Pediatr. 10, 91.

Honey, C.J., Thivierge, J.P., Sporns, O., 2010. Can structure predict function in the human brain? NeuroImage 52, 766–776.

Iturria-Medina, Y., Sotero, R.C., Canales-Rodríguez, E.J., Alemán-Gómez, Y., Melie-García, L., 2008. Studying the human brain anatomical network via diffusion-weighted MRI and graph theory. NeuroImage 40, 1064–1076.

Jarvis, S., Glinianaia, S.V., Torrioli, M.G., Platt, M.J., Miceli, M., Jouk, P.S., Johnson, A., Hutton, J., Hemming, K., Hagberg, G., Dolk, H., Chalmers, J., 2003. Cerebral palsy and intrauterine growth in single births: European collaborative study. Lancet 362, 1106–1111.

Kady, S., Gardosi, J., 2004. Perinatal mortality and fetal growth restriction. Best Pract. Res. Clin. Obstet. Gynaecol. 18, 397–410.

Knickmeyer, R.C., Gouttard, S., Kang, C., Evans, D., Wilber, K., Smith, J.K., Hamer, R.M., Lin, W., Gerig, G., Gilmore, J.H., 2008. A structural MRI study of human brain development from birth to 2 years. J. Neurosci. 28, 12176–12182.

Kobel, M., Bechtel, N., Specht, K., Klarhöfer, M., Weber, P., Scheffler, K., Opwis, K., Penner, I.-K., 2010. Structural and functional imaging approaches in attention deficit/hyperactivity disorder: does the temporal lobe play a key role? Psychiatry Res. 183, 230–236.

Leitner, Y., Fattal-Valevski, A., Geva, R., Eshel, R., Toledano-Alhadef, H., Rotstein, M., Bassan H., Radianu, B., Bitchonsky, O., Jaffa, A.J., Harel, S., 2007. Neurodevelopmental outcome of children with intrauterine growth retardation: a longitudinal, 10-year prospective study. J. Child Neurol. 22, 580–587.

Li, Y., Liu, Y., Li, J., Qin, W., Li, K., Yu, C., Jiang, T., 2009. Brain anatomical network and intelligence. PLoS Comput. Biol. 5, e1000395.

Liu, Y., Liang, M., Zhou, Y., He, Y., Hao, Y., Song, M., Yu, C., Liu, H., Liu, Z., Jiang, T., 2008. Disrupted small-world networks in schizophrenia. Brain 131, 945–961.

Lo, C.Y., Wang, P.N., Chou, K.H., Wang, J., He, Y., Lin, C.P., 2010. Diffusion tensor tractography reveals abnormal topological organization in structural cortical networks in Alzheimer's disease. J. Neurosci. 30, 16876–16885.

Lodygensky, G.A., Seghier, M.L., Warfield, S.K., Tolsa, C.B., Sizonenko, S., Lazeyras, F., Hüppi, P.S., 2008. Intrauterine growth restriction affects the preterm infant's hippocampus. Pediatr. Res. 63, 438–443.

Maes, F., Collignon, A., Vandermeulen, D., Marchal, G., Suetens, P., 1997. Multimodality image registration by maximization of mutual information. IEEE Trans. Med. Imaging 16, 187–198.

Makki, M.I., Govindan, R.M., Wilson, B.J., Behen, M.E., Chugani, H.T., 2009. Altered fronto-striato-thalamic connectivity in children with Tourette syndrome assessed with diffusion tensor MRI and probabilistic fiber tracking. J. Child Neurol. 24, 669–678.

Mallard, C., Loeliger, M., Copolov, D., Rees, S., 2000. Reduced number of neurons in the hippocampus and the cerebellum in the postnatal guinea-pig following intrauterine growth-restriction. Neuroscience 100, 327–333.

Marsal, K., 2002. Intrauterine growth restriction. Curr. Opin. Obstet. Gynecol. 14, 127–135.

McCarton, C.M., Wallace, I.F., Divon, M., Vaughan Jr., H.G., 1996. Cognitive and neurologic development of the premature, small for gestational age infant through age 6: comparison by birth weight and gestational age. Pediatrics 98, 1167–1178.

Michel, V., Gramfort, A., Varoquaux, G., Eger, E., Keribin, C., Thirion, B., 2012. A supervised clustering approach for fMRI-based inference of brain states. Pattern Recognit. 45 (6), 2041–2049.

Padilla, N., Falcon, C., Sanz-Cortes, M., Figueras, F., Bargallo, N., Crispi, F., Eixarch, E., Arranz, A., Botet, F., Gratacos, E., 2011. Differential effects of intrauterine growth restriction on brain structure and development in preterm infants: a magnetic resonance imaging study. Brain Res. 1382, 98–108.

Paus, T., Collins, D.L., Evans, A.C., Leonard, G., Pike, B., Zijdenbos, A., 2001. Maturation of white matter in the human brain: a review of magnetic resonance studies. Brain Res. Bull. 54, 255–266.

Rees, S., Harding, R., Walker, D., 2011. The biological basis of injury and neuroprotection in the fetal and neonatal brain. Int. J. Dev. Neurosci. 29, 551–563.

Robinson, H.P., Fleming, J.E., 1975. A critical evaluation of sonar "crown-rump length" measurements. Br. J. Obstet. Gynaecol. 82, 702–710.

Rubinov, M., Sporns, O., 2009. Complex network measures of brain connectivity: uses and interpretations. NeuroImage 52, 1059–1069.

Scherjon, S., Briet, J., Oosting, H., Kok, J., 2000. The discrepancy between maturation of visual-evoked potentials and cognitive outcome at five years in very preterm infants with and without hemodynamic signs of fetal brain-sparing. Pediatrics 105, 385–391.

Shi, F., Yap, P.T., Wu, G., Jia, H., Gilmore, J.H., Lin, W., Shen, D., 2011. Infant brain atlases from neonates to 1- and 2-year-olds. PLoS One 6, e18746.

Shu, N., Liu, Y., Li, J., Li, Y., Yu, C., Jiang, T., 2009. Altered anatomical network in early blindness revealed by diffusion tensor tractography. PLoS One 4, e7228.

Shu, N., Liu, Y., Li, K., Duan, Y., Wang, J., Yu, C., Dong, H., Ye, J., He, Y., 2011. Diffusion tensor tractography reveals disrupted topological efficiency in white matter structural networks in multiple sclerosis. Cereb. Cortex 21, 2565–2577.

Smyser, C.D., Inder, T.E., Shimony, J.S., Hill, J.E., Degnan, A.J., Snyder, A.Z., Neil, J.J., 2010. Longitudinal analysis of neural network development in preterm infants. Cereb. Cortex 20, 2852–2862.

Smyser, C.D., Snyder, A.Z., Neil, J.J., 2011. Functional connectivity MRI in infants: exploration of the functional organization of the developing brain. NeuroImage 56, 1437–1452.

Sobradillo, B., Aguirre, A., Aresti, U., Bilbao, C., Fernandez-Ramos, C., Lizarraga, A., Lorenzo, H., Madariaga, L., Rica, I., Ruiz, I., Sanchez, E., Santamaria, C., Serrano, J., Zabala, A., Zurimendi, B., Hernandez, M., 2004. Curvas y tablas de crecimiento (Estudios longitudinal y transversal). Fundacion Faustino Orbegozo Eizaguirre Bilbao.

Sporns, O., Tononi, G., 2001. Classes of network connectivity and dynamics. Complexity 7, 28–38.

Sporns, O., Tononi, G., Kotter, R., 2005. The human connectome: a structural description of the human brain. PLoS Comput. Biol. 1, e42.

Studholme, C., Hill, D.L.G., Hawkes, D.J., 1999. An overlap invariant entropy measure of 3D medical image alignment. Pattern Recognit. 32, 71–86.

Thompson, D.K., Warfield, S.K., Carlin, J.B., Pavlovic, M., Wang, H.X., Bear, M., Kean, M.J., Doyle, L.W., Egan, G.F., Inder, T.E., 2007. Perinatal risk factors altering regional brain structure in the preterm infant. Brain 130, 667–677.

Toft, P.B., 1999. Prenatal and perinatal striatal injury: a hypothetical cause of attention-deficit-hyperactivity disorder? Pediatr. Neurol. 21, 602–610.

Tolsa, C.B., Zimine, S., Warfield, S.K., Freschi, M., Sancho Rossignol, A., Lazeyras, F., Hanquinet, S., Pfizenmaier, M., Hüppi, P.S., 2004. Early alteration of structural and functional brain development in premature infants born with intrauterine growth restriction. Pediatr. Res. 56, 132–138.

Tomasi, D., Volkow, N.D., 2011. Functional connectivity hubs in the human brain. NeuroImage 57, 908–917.

Tristan-Vega, A., Arribas, J.I., 2007. A fast B-spline pseudo-inversion algorithm for consistent image registration. Proceedings of the International Conference on Computer Analysis Images and Patterns (CAIP), Vienna, Austria, pp. 768–775.

Tuch, D.S., 2004. Q-ball imaging. Magn. Reson. Med. 52, 1358–1372.

Tzourio-Mazoyer, N., Landeau, B., Papathanassiou, D., Crivello, F., Etard, O., Delcroix, N., Mazoyer, B., Joliot, M., 2002. Automated anatomical labeling of activations in SPM using a macroscopic anatomical parcellation of the MNI MRI single-subject brain. NeuroImage 15, 273–289.

Vourkas, M., Micheloyannis, S., Simos, P.G., Rezaie, R., Fletcher, J.M., Cirino, P.T., Papanicolaou, A.C., 2010. Dynamic task-specific brain network connectivity in children with severe reading difficulties. Neurosci. Lett. 488, 123–128.

Wang, L., Zhu, C., He, Y., Zang, Y., Cao, Q., Zhang, H., Zhong, Q., Wang, Y., 2009. Altered small-world brain functional networks in children with attention-deficit/hyperactivity disorder. Hum. Brain Mapp. 30, 638–649.

Wang, L., Metzak, P.D., Honer, W.G., Woodward, T.S., 2010. Impaired efficiency of functional networks underlying episodic memory-for-context in schizophrenia. J. Neurosci. 30, 13171–13179.

Wang, Q., Su, T.P., Chou, K.H., Chen, I.Y., Jiang, T., Lin, C.P., 2012. Anatomical insights into disrupted small-world networks in schizophrenia. NeuroImage 59, 1085–1093.

Warfield, S.K., Guimond, A., Roche, A., Bharatha, A., Tei, A., Talos, F., Rexilius, J., Ruiz-Alzola, J., Westin, C.F., Haker, S., Angenent, S., Tannenbaum, A., Jolesz, F., Kilkinis, R., 2002. Advanced nonrigid registration algorithms for image fusion. In: Mazziotta, J.C., Toga, A.W. (Eds.), Brain Mapping: The Methods. Elsevier, pp. 661–690.

Watts, D.J., Strogatz, S.H., 1998. Collective dynamics of 'small-world' networks. Nature 393, 440–442.

Wedeen, V.J., Hagmann, P., Tseng, W.Y., Reese, T.G., Weisskoff, R.M., 2005. Mapping complex tissue architecture with diffusion spectrum magnetic resonance imaging. Magn. Reson. Med. 54, 1377–1386.

Wee, C.Y., Yap, P.T., Li, W., Denny, K., Browndyke, J.N., Potter, G.G., Welsh-Bohmer, K.A., Wang, L., Shen, D., 2010. Enriched white matter connectivity networks for accurate identification of MCI patients. NeuroImage 54, 1812–1822.

Wen, W., Zhu, W., He, Y., Kochan, N.A., Reppermund, S., Slavin, M.J., Brodaty, H., Crawford, J., Xia, A., Sachdev, P., 2011. Discrete neuroanatomical networks are associated with specific cognitive abilities in old age. J. Neurosci. 31, 1204–1212.

Wu, T., Wang, L., Chen, Y., Zhao, C., Li, K., Chan, P., 2009. Changes of functional connectivity of the motor network in the resting state in Parkinson's disease. Neurosci. Lett. 460, 6–10.

Yan, C., Gong, G., Wang, J., Wang, D., Liu, D., Zhu, C., Chen, Z.J., Evans, A., Zang, Y., He, Y., 2010. Sex- and brain size-related small-world structural cortical networks in young adults: a DTI tractography study. Cereb. Cortex 21, 449–458.

Yap, P.T., Fan, Y., Chen, Y., Gilmore, J.H., Lin, W., Shen, D., 2011. Development trends of white matter connectivity in the first years of life. PLoS One 6, e24678.